nature communications

Article

https://doi.org/10.1038/s41467-024-55512-3

Two-dimensional anion-rich $NaCl_2$ crystal under ambient conditions

Received: 8 May 2023

Accepted: 10 December 2024

Published online: 07 January 2025

Check for updates

Ruobing Yi[1,2,3,8], Jie Jiang[1,8] ✉, Yizhou Yang[4,8], Yueyu Zhang[5] ✉, Siyan Gao[4], Yimin Zhao[2], Jiahao Hu[1], Xuchang Su[2], Xinming Xia[1], Bingquan Peng[5], Fangfang Dai[5], Pei Li[1], Zhao Guan[6], Haijun Yang[7], Fangyuan Zhu[7], Jiefeng Cao[7], Zhe Wang[2], Haiping Fang[4,5], Lei Zhang[2] ✉ & Liang Chen[1] ✉

The two-dimensional (2D) "sandwich" structure composed of a cation plane located between two anion planes, such as anion-rich CrI_3, VS_2, VSe_2, and $MnSe_2$, possesses exotic magnetic and electronic structural properties and is expected to be a typical base for next-generation microelectronic, magnetic, and spintronic devices. However, only a few 2D anion-rich "sandwich" materials have been experimentally discovered and fabricated, as they are vastly limited by their conventional stoichiometric ratios and structural stability under ambient conditions. Here, we report a 2D anion-rich $NaCl_2$ crystal with sandwiched structure confined within graphene oxide membranes with positive surface potential. This 2D crystal has an unconventional stoichiometry, with Na:Cl ratio of approximately 1:2, resulting in a molybdenite-2H-like structure with cations positioned in the middle and anions in the outer layer. The 2D $NaCl_2$ crystals exhibit room-temperature ferromagnetism with clear hysteresis loops and transition temperature above 320 K. Theoretical calculations and X-ray magnetic circular dichroism (XMCD) spectra reveal the ferromagnetism originating from the spin polarization of electrons in the Cl elements of these crystals. Our research presents a simple and general approach to fabricating advanced 2D unconventional stoichiometric materials that exhibit half-metal and ferromagnetism for applications in electronics, magnetism, and spintronics.

Since the discovery of intrinsic ferromagnetism in two-dimensional (2D) materials[1,2], crystals with these properties have attracted considerable attention and have been studied with theory and experimental synthesis[3–5], showing potential for a variety of applications such as sensing and data storage. A common structural feature of all these 2D crystals is typically an anion-rich 'sandwich' conformation, which can be regarded as a single sandwiched anion-cation-anion layer[6], such as VSe_2[3], VS_2[7], $MnSe_2$[4], VI_3[5], and chromium tellurides[8–10]. In such an

[1]School of Physical Science and Technology, Ningbo University, Ningbo, China. [2]MOE Key Laboratory for Nonequilibrium Synthesis and Modulation of Condensed Matter, School of Physics, Xi'an Jiaotong University, Xi'an, China. [3]School of Chemistry and Chemical Engineering, Shandong University of Technology, Zibo, China. [4]School of Physics, East China University of Science and Technology, Shanghai, China. [5]Wenzhou Institute, University of Chinese Academy of Sciences, Wenzhou, Zhejiang, China. [6]Key Laboratory of Polar Materials and Devices (MOE) and Department of Electronics, East China Normal University, Shanghai, China. [7]Shanghai Synchrotron Radiation Facility, Shanghai Advanced Research Institute, Chinese Academy of Sciences, Shanghai, China. [8]These authors contributed equally: Ruobing Yi, Jie Jiang, Yizhou Yang. ✉e-mail: jiangjie1@nbu.edu.cn; zhangyy@wiucas.ac.cn; zhangleio@xjtu.edu.cn; liangchen@zafu.edu.cn

anion-rich 'sandwich' structure, interlayer interactions between two neighboring ion layers are weakened by repulsive Coulomb forces between negatively charged ions that face each other in adjacent layers, allowing them to be stabilized as a single or two layers[11]. Taking the case of two-dimensional chromium tellurides, they have exhibited immense promise in the realm of compact spintronic device applications, primarily due to their natural ferromagnetic properties maintained at room temperature[8–10].

Recently, some anomalous structures of metal halide salt crystals have been experimentally discovered, exhibiting properties including piezoelectricity[12], piezoresistance[13], metallicity and room-temperature ferromagnetism[14]. These findings present possibilities for developing materials with unique properties. However, investigations regarding alkali metal chlorides in the context of the 2D anion-rich "sandwich" conformation have not been reported. This absence of research can be attributed to the significant challenges posed by achieving the appropriate stoichiometric ratios and maintaining structural stability under ambient conditions[15].

In this work, we experimentally prepared stable 2D anion-rich $NaCl_2$ crystals with a Na:Cl average ratio of ~1:2 under ambient conditions in graphene oxide membranes with controlled positive surface potential (p-GO). Such $NaCl_2$ crystals, which we refer to as "sodium dichloridene", were directly observed by high-resolution transmission electron microscopy (HR-TEM). The 2D $NaCl_2$ crystals showed a hexagonal layer with a molybdenite-2H-like structure, which can be interpreted as a layer of positively charged sodium cations sandwiched by two layers of negatively charged chloride anions. The extended X-ray absorption fine structure (EXAFS) and X-ray absorption near edge structure (XANES) results revealed that this Na-Cl crystal has distinctive bond lengths and local environments, which differ from those of regular NaCl crystals. Importantly, the ferromagnetism of the $NaCl_2$ crystals at room temperature was detected experimentally. Moreover, compared with pristine p-GO and NaCl, the $NaCl_2$ crystals showed enhanced electrical conductivity. Density Functional Theory (DFT) and X-ray magnetic circular dichroism (XMCD) spectra reveal the ferromagnetism originating from the spin polarization of electrons in the Cl elements of these crystals. This property arises from the full occupancy of one spin channel near the Fermi level due to the *p* electrons of the chloride anions, while the other channel remains empty, which distinguishes it from the properties usually observed in most transition metal chalcogenides. These findings are critical for understanding and synthesizing various 2D anion-rich "sandwich" crystals with unique properties that could be universally applied in the fields of microelectronics, magnetism[14,16], and spintronics[15].

Results

p-GO suspension was prepared by functionalizing GO flakes with polyethyleneimine (PEI). This modulated the zeta (ζ) potential to approximately +36 mV from the original negatively charged surface in a neutral environment (see Methods and Supplementary Information section PS1). Freestanding p-GO membranes were prepared from the p-GO suspension by the drop-casting method[13,14]. According to the C1s and N1s XPS results of p-GO (Fig. S2), the positively charged -NH_3^+ group was successfully introduced to the surface of GO flakes[17–21]. The obtained p-GO membranes were then immersed in 3 mol L^{-1} (M) NaCl solution overnight under ambient conditions (25 °C and 1 atm), followed by centrifugation to remove the free solution and drying at 70 °C under vacuum conditions for 12 h.

The Na–Cl crystals inside p-GO (Na–Cl@p-GO) membranes were analysed by transmission electron microscopy (TEM). The samples were prepared by manually exfoliating the Na–Cl@p-GO membranes to ultrathin slices[14]. Due to the sensitivity of the Na–Cl crystals to electron beam irradiation and electron beam damage, TEM imaging was performed in the low-dose mode with short exposure times within 0.2 s. As a result, the clear and random distribution of Na–Cl crystalline regions with submicron size in an ultrathin p-GO membrane was observed using the high-angle annular dark field scanning TEM (HADDF-STEM) mode (Fig. 1b). The high-resolution TEM (HR-TEM) image in Fig. 1c(i) and S3d-e show that the Na–Cl crystals exhibit a honeycomb lattice with an average lattice constant of 3.20 ± 0.23 Å, different from the lattice of graphene. Two fast Fourier transform (FFT) patterns were obtained from the magnified image in Fig. 1c(ii), corresponding to the first-order reflections of $NaCl_2$ and p-GO crystals, respectively. The FFT analyses of the Na–Cl lattice yielded a hexagonal lattice with first-order maximal points at (1 ± 0.03)/7.22 nm^{-1}, which is different from the lattice of graphene. In most cases, such Na–Cl crystals usually present single-crystal structures (Fig. S4 and S5a), together with relatively fewer double-oriented crystals that have the same hexagonal lattice with a twisted angle of about 30° between them (Fig. S6).

The atomic ratios of the Na and Cl of these Na–Cl crystals were measured by TEM energy-dispersive X-ray spectroscopy (EDS) analysis. The analysis shows that more than half of the regions have significantly more Cl ions than Na ions, resulting in statistical ratios mainly concentrated around ~1:1 and ~1:2 for Na:Cl (Fig. 1d and Supplementary Information section PS4). The ratio of Na to Cl elements was further confirmed by X-ray photoelectron spectroscopy (XPS) (Fig. S17). The result shows that the ratios of Na to Cl are mainly distributed between 0.5 and 1, indicating that anion-rich $NaCl_2$ and regular NaCl crystals were simultaneously present, consistent with the TEM results. In addition, the regulation of the NaCl solution concentration utilized in immersing p-GO will influence the ratio of Na and Cl (Fig. S10–S13). With increasing NaCl concentration from 0.03 M to 3 M, the regions where the ratio of Na to Cl ions is 1:2 gradually increase, indicating a corresponding increase of $NaCl_2$ in p-GO membranes. When the concentration of NaCl was increased to 3 M, it showed that there were still more than half of the regions had significantly more Cl ions than Na ions, resulting in statistical ratios mainly concentrated around ~1:1 and ~1:2 for Na:Cl. Such a distribution indicates that both the Na–Cl and regular NaCl crystals are present simultaneously, which is verified by the synchrotron Na and Cl K-edge XANES spectra (details in Supplementary Information section PS6). Importantly, considering all exotic crystals with unconventional stoichiometries, this study provided the first confirmed existence of 2D anion-rich $NaCl_2$ crystals under ambient conditions.

It is an anion-rich 'sandwich' structure with Na atoms in the middle and Cl atoms in the outer layer. Global optimization searches[22] together with DFT calculations were applied to study the crystal structure of $NaCl_2$. Many different $(NaCl_2)_n$ ($n \le 4$) cells were enumerated in the structural searching, and the final stable structures were selected by comparing their total energies (see Supplementary Information section PS8). The top and side views of Fig. 2a show the structure of $NaCl_2$ obtained from our research, and this structure is both energetically favorable and close to the experimental result. The optimized lattice parameters are $a = b = 3.29$ Å with these two lattice vectors oriented 120° to each other, well consistent with the TEM results (Fig. 1c). The Na–Cl bond length in $NaCl_2$ Crystals is ~2.71 Å (The atomic coordination file is presented in Supplementary Information section PS8), which is shorter than the ~2.81 Å in regular NaCl crystals (Fig. S5b), as confirmed by synchrotron EXAFS analysis (See Supplementary Information section PS7). It is a molybdenite-2H-like structure with a hexagonal $P\bar{6}m2$ (187) space group, in the form of a hexagonal plane of Cl atoms on two sides of a hexagonal plane of Na atoms. Electron localization function[23] computation (Fig. 2a) shows a "bell"-shaped localization over the Cl atom, indicating the polarization by the ionic bond between Na and Cl. The results confirm the existence of 2D $NaCl_2$ crystals with an anion-rich 'sandwich' structure.

This unconventional structure of $NaCl_2$ crystals induces ferromagnetism at room-temperature. We measured the magnetization curves ($M-H$) as a function of the applied magnetic field for the

https://doi.org/10.1038/s41467-024-55512-3

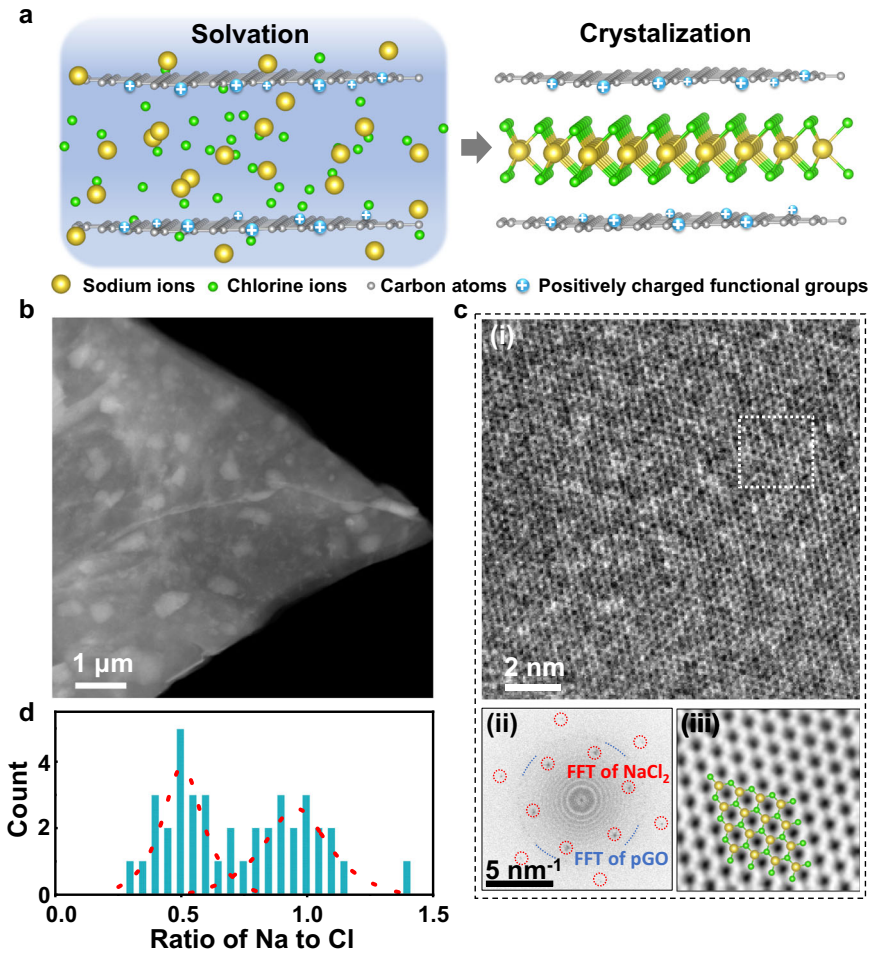

Fig. 1 | Two-dimensional (2D) $NaCl_2$ crystal with sandwiched structure in graphene oxide membranes with positive surface potential (p-GO). a Schematic design of a p-GO membrane with a positively charged surface prepared by functionalizing GO with polyethyleneimine (PEI). The surface of p-GO exhibits a more favorable attraction to Cl^- than to Na^+. **b** Dark-field transmission electron microscopy (TEM) images of ultrathin Na–Cl@p-GO membranes. **c** (i) High-resolution TEM (HR-TEM) of $NaCl_2$ single crystal; (ii) Fast Fourier transform (FFT) of the entire bright-field image (FFT of $NaCl_2$ and p-GO are marked by red dashed lines and blue dashed lines, respectively); and (iii) inverse FFT (iFFT) of the localized area, showing a hexagonal lattice pattern with six first-order maxima points at $(1 \pm 0.03)/7.22\ nm^{-1}$. **d** Ratios of Na to Cl in p-GO membranes determined by TEM energy-dispersive X-ray spectroscopy (EDS) (details in Supplementary Information section PS4). The red dashed line is the fit of the distribution of rations.

Na–Cl@p-GO system at T = 300 K using Magnetic Property Measurement System (MPMS-3, Quantum Design) (Fig. 3a). A strongly enhanced ferromagnetism was observed in Na–Cl@p-GO with a saturation magnetic moment (M_s) of 0.63 emu/g, which is about three times the M_s of p-GO (0.20 emu/g). The magnetic hysteresis loops of Na–Cl@p-GO were further measured at various temperatures ranging from 260 to 340 K (Fig. 3b). As the temperature increases over 320 K, the coercivity gradually shrinks and almost disappears. The results confirm that the room-temperature ferromagnetism in $NaCl_2$ crystals is validated as the transition temperature is above 320 K. We note that the possible contamination of Fe, Co, and Ni in Na–Cl@p-GO was negligibly small as low cation concentrations below the detection limits, according to the XPS and synchrotron X-ray absorption spectroscopy (XAS) results (see Supplementary Information section PS5). We performed additional measurements of the concentrations of Fe, Co, and Ni in our samples using inductively coupled plasma mass spectrometry (ICP-MS), with a precision of up to ppb. The concentrations of Fe, Co, and Ni in our samples were 48.8, 1.5, and 15.0 $\mu g\ g^{-1}$, respectively. Therefore, the magnetic signals produced by the contaminations were negligibly small. In addition, the resistivities of Na–Cl@p-GO have a smaller resistance, which is decreased by about two orders of magnitude than that of p-GO (Fig. 3c), indicating a unique electronic property of $NaCl_2$, consistent with our DFT results (details see Supplementary Information section PS10). Taking into account the aromatic surface induction[24], this metallic properties of $NaCl_2$ can be extended onto the p-GO substrate to improve the conductivity.

Discussion

It was surprising that the $NaCl_2$ crystals exhibited room-temperature ferromagnetism, because they were composed of only Na and Cl elements, which are believed to be nonmagnetic conventionally. Using a spin-polarized DFT calculation[25–27], we revealed that the magnetic ground state of the $NaCl_2$ is ferromagnetic (Fig. 2b and Table S4). All the spin momentums are localized on Cl atoms, with 0.5 μB on each of the Cl atoms. This is consistent with the spin charge density plot in Fig. 2c, showing that both spin channels have contributions from the electrons on the Cl atom. From the spin-polarized band and density of state calculation, the Fermi level of the spin-down channel was fully occupied while that of the spin-up channel was unoccupied, indicating that $NaCl_2$ is metallic only on one spin channel and insulating on the other one. This half occupation that was contributed by the *p*-orbitals in Cl (Fig. 2d) is very different from that of conventional ferromagnetic materials, such as Fe, Co, and Ni, where the magnetism originates from

https://doi.org/10.1038/s41467-024-55512-3

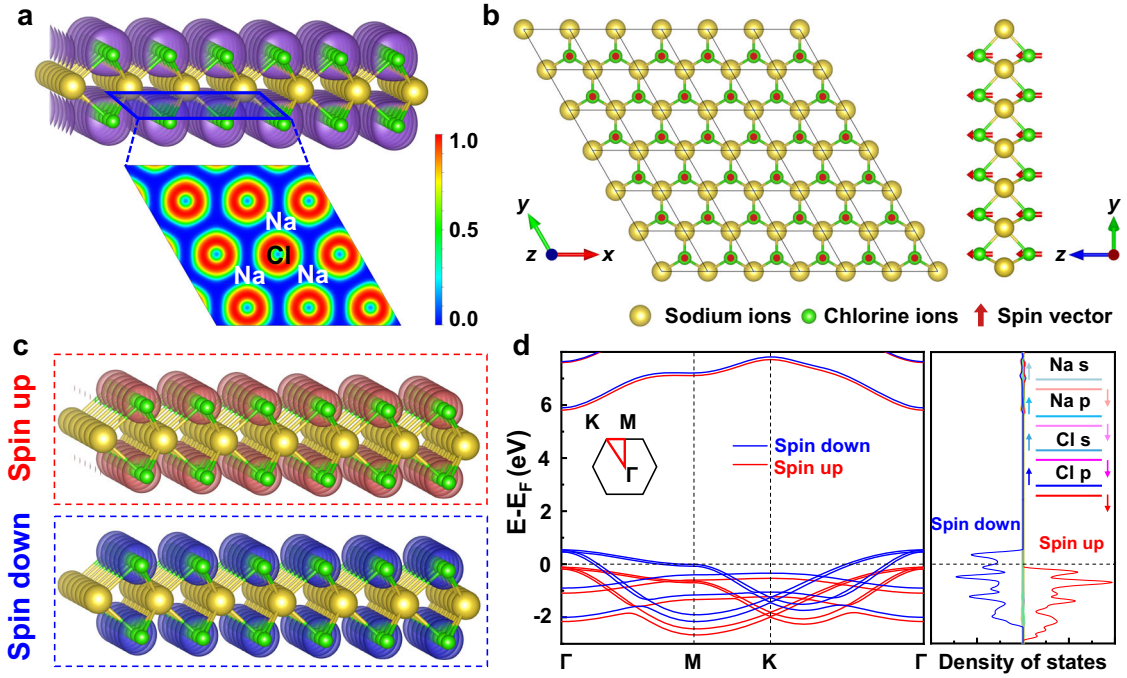

Fig. 2 | Theoretical computations of crystal structure, electronic structural and magnetic properties for $NaCl_2$ crystal. a Electron localization function for $NaCl_2$ with an isosurface of 0.4 (upper) and a 2D projection on the chloride plane. Purple spheres represents the electron density of chloride ions. **b** Schematic diagram of the ferromagnetic ground state of $NaCl_2$, where the red arrows present the spin alignment. **c** Spin charge density of $NaCl_2$ crystal with an isosurface of 0.03 e for both spin directions. Red and blue spheres represent spin density for spin up channels and spin down channels, repectively. **d** Spin-polarized band and density of states (DOSs) of $NaCl_2$.

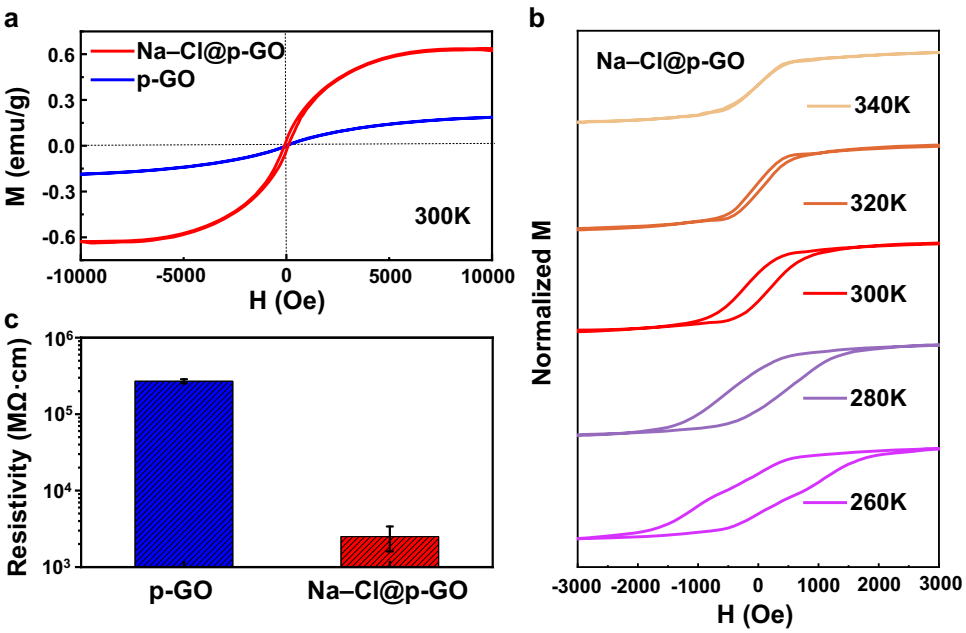

Fig. 3 | Room-temperature ferromagnetism and electrical conductivity of the Na–Cl@p-GO membrane. a Magnetization hysteresis loops of Na–Cl@p-GO membranes (red curve) and p-GO membranes (blue curve) measured at room temperature (the magnetic field is set to be perpendicular to the surface of membranes). **b** Magnetization hysteresis loops of Na–Cl@p-GO membranes at the temperature range from 260 to 340 K. **c** The resistivity measurement with two electrodes connecting with the up and down surfaces of p-GO and Na–Cl@p-GO membranes, respectively, under ambient conditions. Error bars indicate the standard deviation from 15 different areas from three samples (details in Supplementary Table S5).

the *d*-orbitals. The spin-resolved DFT calculation revealed that the $NaCl_2$ crystal is a half-metal, which is expected for spintronic devices[28].

The magnetic force microscope (MFM) measurements observed the magnetic signals of the crystal domains inside the Na–Cl@p-GO membranes. The atomic force microscopy (AFM) image in Fig. 4a shows a topography of the Na–Cl@p-GO membrane surface. The corresponding MFM image was obtained in the same region (Fig. 4b), with a lift scan height of 20 nm from the topographic scanning of AFM, where the van-der-Waals force do not interfere the magnetic force[29,30]. The MFM tip was magnetized in the direction that pointed into the

https://doi.org/10.1038/s41467-024-55512-3

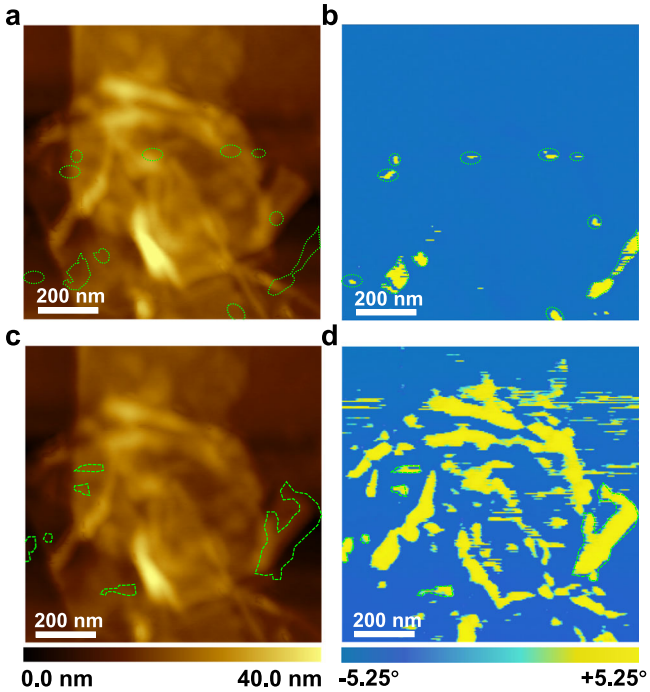

Fig. 4 | Topographic and magnetic force microscope (MFM) measurements of Na–Cl@p-GO membrane at room temperature. Atomic force microscopy (AFM) images (**a**, **c**) and MFM images (**b**, **d**) in the same area of Na–Cl@p-GO membrane on the silicon wafer. The MFM tip was magnetized into the Na–Cl@p-GO surface (**b**) and out of the Na–Cl@p-GO surface (**d**), respectively.

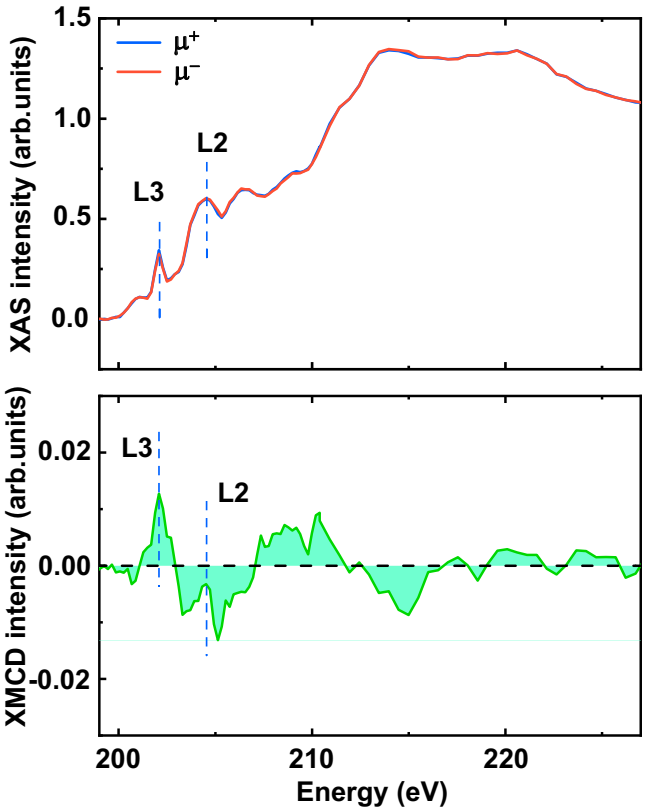

Fig. 5 | X-ray absorption spectroscopy (XAS) and X-ray magnetic circular dichroism (XMCD) spectra of Cl $L_{2,3}$ at room temperature. The top is Cl $L_{2,3}$ XAS of the Na–Cl@p-GO membranes measured with left-circularly (μ^+) and right-circularly (μ^-) polarized light, and the bottom is the corresponding XMCD spectrum (i.e., $\mu^+ - \mu^-$).

membrane surface. As shown in Fig. 4b, several magnetic domains marked by the green dashed line appear. It exhibited no relationship with the AFM image and is decoupled from the topographic signal, demonstrating the presence of magnetic domains in the Na–Cl@p-GO membrane.

Then, the MFM tip was magnetized in an opposite direction pointing out of the membrane surface, and more magnetic domains were obtained in the same region (Fig. 4d). Due to the reversed magnetization direction of the MFM tip, the distribution changes in the magnetic domains indicate a sensitive magnetic property of the Na–Cl@p-GO membrane. We note that these magnetic domains do not align with the magnetic characteristics arising from graphene defects[31], which are primarily striped and distributed along the edges and exhibit a dark phase contrast upon the reversal of the magnetization direction of the MFM tip. The results reveal that the distribution of magnetic domains is in parts of the Na–Cl crystal regions, indicating the coexistence of the Na–Cl and regular NaCl crystals. In addition, the regions of p-GO membrane stacking and ripples (which exhibit a height difference in the topographic scanning) will facilitate the adsorption and accommodation of Na–Cl crystals within them[32]. This will lead to a certain correlation between the topography in AFM and the distribution of magnetic signals in MFM images. Therefore, the MFM results indicate the presence of magnetic domains resulting from the Na–Cl crystals located within the p-GO membranes.

The magnetic moments originating from Cl elements in Na–Cl crystals, were further verified through XMCD measurements. XAS of $L_{2,3}$ edges of Cl (199–227 eV), were measured using left-circularly (μ^+) and right-circularly (μ^-) polarized light at a 0.6 T magnet and 25 °C, on beam line BL07U at Shanghai Synchrotron Radiation Facility. The XMCD signal was obtained by subtracting XAS of the μ^+ and μ^- polarized light. Measurements used total-electron-yield (TEY) detection, where the drain current was taken from the sample to the ground.

Figure 5 shows the XAS and XMCD spectra at Cl $L_{2,3}$ edges for Na–Cl@p-GO membrane. The peaks at 202.1 eV and 204.3 eV correspond to the L_3 and L_2 edges of Cl[33]. The X-ray absorption spectra at the Cl $L_{2,3}$ edge taken with different photon helicities showed an obvious difference, and the XMCD spectrum presented the negative and positive peaks at the location of L_2 and L_3 (Fig. 5). This result suggests the spin polarization of electrons of Cl elements in the Na–Cl@p-GO membrane, revealing the ferromagnetic properties of $NaCl_2$ crystals, which is consistent with our theoretical predictions.

Note that, relative to the anion-rich $NaCl_2$ with an exotic intrinsic half-metallicity and ferromagnetism, the cation-rich Na_2Cl crystals discussed in our previous reports may have unusual electronic and magnetic properties, while the rock salt NaCl, the simplest compound, is insulating. These recently discovered crystals are anion rich or cation rich, and their formation mechanism can be mainly attributed to both the ion-π interaction[32,34,35] and the confined space[16,36]. For those π-conjugated systems with negative surface potential[32,35], cations are more likely to be absorbed on them than anions and vice versa. In addition, similar anion-rich crystals were also observed when we incubated the p-GO membranes with KCl solutions (Supplementary Information section PS11 and PS12), demonstrating a simple but universal approach to fabricating 2D unconventional stoichiometric materials with alkali metal halides.

In summary, we experimentally fabricated stable 2D anion-rich $NaCl_2$ crystals with room-temperature ferromagnetism under ambient conditions using p-GO membranes with positive surface potential as a substrate. Theoretical calculations and XMCD measurements revealed that the unique ferromagnetism is originating from the spin

polarization of electrons in the Cl elements of these crystals. Stoichiometric control of the alkali metal halide crystals using π-conjugated systems, with a modulated surface potential to induce specific functions, opens a new field for material design. The exploration of these exotic crystals deepens the understanding of crystallization under ambient conditions, and their unique properties due to the allosteric effect may have great potential application in the fields of microelectronics, magnetism, and spintronics.

Methods

Fabrication of freestanding positive graphene oxide (p-GO) membranes

The GO suspension was prepared from graphite powders according to Hummer's method, as mentioned in previous reports[32]. At room temperature, 500 µL of 1-(3-Dimethylaminopropyl)−3-ethylcarbodiimide (EDC) was added to 60 mL GO solution (2 mg L^{-1}), and the reaction was carried out under continuous stirring for 1 h[37,38]. Next, 0.2 g of polyethylene imine (PEI) was added to the obtained solution, and the reaction was continued for another 3 h with stirring. Then, the reaction-mixed solution was dialyzed for one week to remove residual reactants. Finally, the obtained suspension was diluted to 1 mg mL^{-1} by deionized water. Freestanding p-GO membranes were fabricated by drop-casting the p-GO suspension (1 mg mL^{-1}, 1 ml) droplets onto a smooth paper substrate after drying at 70 °C for 12 h[34].

Characterization

The high-resolution TEM micrographs and SAED images were acquired at room temperature by FEI F200C TEM operating at 200-kV; High-angle annular dark field scanning TEM (HADDF-STEM) and energy-dispersive X-ray spectroscopy (EDS) were performed by a Talos F200X (S)TEM operating at 200-kV; The XPS of Na−Cl@p-GO membrane was characterized by a Thermo Fisher ESCALAB Xi+ system; XRD patterns of GO and p-GO membranes were obtained by an X-ray diffractometer system (Bruker D8 Advance). The magnetic properties of the Na−Cl@p-GO membranes and pure p-GO membranes with respect to temperature and field were measured using a quantum design MPMS-3. The AFM and MFM images were obtained with a commercial AFM system (Asylum Research Cypher of Oxford). For MFM detection, ultrathin and small Na-Cl@p-GO membrane flakes with a thickness of less than 50 nm were prepared from the p-GO suspension by vacuum filtration, and then transferred to a cleaned silicon wafer substrate; The XMCD, EXAFS and XANES measurements were collected on beam line BL07U, BL14W1, and BL16U1 of the Shanghai Synchrotron Radiation Facility. Before testing, the samples need to be reduced at 120 °C for 2 h to ensure good electrical conductivity; The precision analysis of the elemental composition of our samples was characterized using a inductively coupled plasma mass spectrometry (ICP-MS) (NexION 300X).

Density functional theory (DFT) calculation

In this work, our studies were based on the DFT method for structural relaxation and electronic structure calculation. The ion-electron interaction was treated by the projector augmented-wave technique[39], as implemented in the Vienna ab initio simulation package[40]. The exchange-correlation potential was treated using the Perdew-Burke-Ernzerhof[41] functional. The basis set cut off was 800 eV. The K-mesh was generated by the Monkhorst-Pack scheme[42], and the density of K-points was approximately 0.04 $Å^{-1}$. The Tkatchenko and Scheffler (TS) method[43] was applied to describe the van der Waals interaction.

Differential evolution (DE)-based global optimization method for 2D material design

For details, see Supplementary Information section PS8.

Data availability

The authors declare that all the data supporting the findings of this study are available within the article (and its Supplementary Information file), or available from the corresponding author on request. Source data are provided with this paper.

References

1. Gong, C. et al. Discovery of intrinsic ferromagnetism in two-dimensional van der Waals crystals. *Nature* **546**, 265–269 (2017).
2. Huang, B. et al. Layer-dependent ferromagnetism in a van der waals crystal down to the monolayer limit. *Nature* **546**, 270–273 (2017).
3. Bonilla, M. et al. Strong room-temperature ferromagnetism in VSe_2 monolayers on van der Waals substrates. *Nat. Nanotechnol.* **13**, 289–293 (2018).
4. O'Hara, D. J. et al. Room temperature intrinsic ferromagnetism in epitaxial manganese selenide films in the monolayer limit. *Nano Lett.* **18**, 3125–3131 (2018).
5. Tian, S. et al. Ferromagnetic van der Waals Crystal VI_3. *J. Am. Chem. Soc.* **141**, 5326–5333 (2019).
6. He, Z. & Que, W. Molybdenum disulfide nanomaterials: structures, properties, synthesis and recent progress on hydrogen evolution reaction. *Appl. Mater. Today* **3**, 23–56 (2016).
7. Zhou, J. et al. Heterodimensional superlattice with in-plane anomalous Hall effect. *Nature* **609**, 46–51 (2022).
8. Meng, L. et al. Anomalous thickness dependence of Curie temperature in air-stable two-dimensional ferromagnetic 1T-$CrTe_2$ grown by chemical vapor deposition. *Nat. Commun.* **12**, 809 (2021).
9. Tang, B. et al. Phase engineering of Cr_5Te_8 with colossal anomalous Hall effect. *Nat. Electron.* **5**, 224–232 (2022).
10. Zhang, X. et al. Room-temperature intrinsic ferromagnetism in epitaxial $CrTe_2$ ultrathin films. *Nat. Commun.* **12**, 2492 (2021).
11. Li, Y. et al. Transient optical modulation of two-dimensional materials by excitons at ultimate proximity. *ACS Nano* **15**, 5495–5501 (2021).
12. Peng, B. et al. Unexpected piezoresistive effect, room-temperature ferromagnetism, and thermal stability of 2D β-CuI crystals in reduced graphene oxide membrane. *Adv. Electron. Mater.* **9**, 2201241 (2023).
13. Xia, X. et al. High-yield synthesis of sodium chlorides of unconventional stoichiometries. *Adv. Mater.* **35**, 2303072 (2023).
14. Zhang, L. et al. Novel 2D CaCl crystals with metallicity, room-temperature ferromagnetism, heterojunction, piezoelectricity-like property and monovalent calcium ions. *Natl Sci. Rev.* **8**, waa274 (2020).
15. Zhang, W. et al. Unexpected stable stoichiometries of sodium chlorides. *Science* **342**, 1502–1505 (2013).
16. Zhao, Y. et al. Graphitic-like hexagonal phase of alkali halides in quasi-two-dimensional confined space under ambient conditions. *ACS Nano* **16**, 2046–2053 (2022).
17. Zhang, M. et al. Controllable ion transport by surface-charged graphene oxide membrane. *Nat. Commun.* **10**, 1–8 (2019).
18. Stankovich, S. et al. Synthesis of graphene-based nanosheets via chemical reduction of exfoliated graphite oxide. *Carbon* **45**, 1558–1565 (2007).
19. Tong, W. et al. Achieving significantly enhanced dielectric performance of reduced graphene oxide/polymer composite by covalent modification of graphene oxide surface. *Carbon* **94**, 590–598 (2015).
20. Liu, H. et al. In situ synthesis of the reduced graphene oxide–polyethyleneimine composite and its gas barrier properties. *J. Mater. Chem. A* **1**, 3739–3746 (2013).
21. Wang, X. et al. 3D self-assembly polyethyleneimine modified graphene oxide hydrogel for the extraction of uranium from aqueous solution. *Appl. Surf. Sci.* **426**, 1063–1074 (2017).

22. Zhang, Y. et al. Inverse design of materials by multi-objective differential evolution. *Comput. Mater. Sci.* **98**, 51–55 (2015).
23. Silvi, B. & Savin, A. Classification of chemical bonds based on topological analysis of electron localization functions. *Nature* **371**, 683–686 (1994).
24. Heimel, G. et al. Charged and metallic molecular monolayers through surface-induced aromatic stabilization. *Nat. Chem.* **5**, 187–194 (2013).
25. Serr, A. & Netznetz, R. R. Polarizabilities of hydrated and free ions derived from DFT calculations. *Int. J. Quantum Chem.* **106**, 2960–2974 (2006).
26. Xu, H. et al. Porous-structured Cu_2O/TiO_2 nanojunction material toward efficient CO_2 photoreduction. *Nanotechnology* **25**, 165402 (2014).
27. Perdew, J. P. & Zunger, A. Self-interaction correction to density-functional approximations for many-electron systems. *Phys. Rev. B* **23**, 5048–5079 (1981).
28. Mishra, S. et al. Topological frustration induces unconventional magnetism in a nanographene. *Nat. Nanotechnol.* **15**, 22–28 (2020).
29. Zhang, G. et al. Above-room-temperature strong intrinsic ferromagnetism in 2D van der waals Fe_3GaTe_2 with large perpendicular magnetic anisotropy. *Nat. Commun.* **13**, 5067 (2022).
30. Zhang, H. et al. Room-temperature skyrmion lattice in a layered magnet $(Fe_{0.5}Co_{0.5})_5GeTe_2$. *Sci. Adv.* **8**, eabm7103 (2022).
31. Červenka, J. et al. Room-temperature ferromagnetism in graphite driven by two-dimensional networks of point defects. *Nat. Phys.* **5**, 840–844 (2009).
32. Chen, L. et al. Ion sieving in graphene oxide membranes via cationic control of interlayer spacing. *Nature* **550**, 380–383 (2017).
33. Kasrai, M. et al. X-ray-absorption near-edge structure of alkali halides: the interatomic-distance correlation. *Phys. Rev. B* **43**, 1763–1772 (1991).
34. Shi, G. et al. Two-dimensional Na–Cl crystals of unconventional stoichiometries on graphene surface from dilute solution at ambient conditions. *Nat. Chem.* **10**, 776–779 (2018).
35. Shi, G. et al. Ion enrichment on the hydrophobic carbon-based surface in aqueous salt solutions due to cation-π interactions. *Sci. Rep.* **3**, 1–5 (2013).
36. Mustonen, K. et al. Toward exotic layered materials: 2D cuprous iodide. *Adv. Mater.* **34**, 2106922 (2022).
37. Zhang, X. et al. Rectified ion transport through 2D nanofluidic heterojunctions. *Phys. Status Solidi RRL* **13**, 1900129 (2019).
38. Quan, D. et al. Laterally heterogeneous 2D layered materials as an artificial light-harvesting proton pump. *Adv. Funct. Mater.* **30**, 2001549 (2020).
39. Blöchl, P. E. Projector augmented-wave method. *Phys. Rev. B* **50**, 17953–17979 (1994).
40. Kresse, G. & Hafner, J. Ab initio molecular-dynamics simulation of the liquid-metal–amorphous-semiconductor transition in germanium. *Phys. Rev. B* **49**, 14251–14269 (1994).
41. Perdew, J. P. et al. Generalized gradient approximation made simple. *Phys. Rev. Lett.* **77**, 3865–3868 (1996).
42. Monkhorst, H. J. & Pack, J. D. Special points for brillouin-zone integrations. *Phys. Rev. B* **13**, 5188–5192 (1976).
43. Tkatchenko, A. & Scheffler, M. Accurate molecular van der waals interactions from ground-state electron density and free-atom reference data. *Phys. Rev. Lett.* **102**, 073005 (2009).

Acknowledgements

This work was supported by the National Natural Science Foundation of China (12074341, 11922410, 12204171, U1832150), the Scientific Research and Developed Funds of Ningbo University (No. ZX2022000015). We thank the staff from BL07U, BL14W1, and BL16U1 beamline of Shanghai Synchrotron Radiation Facility (SSRF) for assistance of XMCD/XAFS data collection.

Author contributions

L.C. and L.Z. conceived the ideas. L.C., Y.Z., L.Z., H.F., R.Y., and J.J. designed the experiments, simulations and co-wrote the manuscript. R.Y., J. J., Y.Z., J. H., X.S., X.X., B.P., F.D., P.L., Z.G., H.Y., F.Z., J.C., and Z.W. performed the experiments and prepared the data graphs. Y.Y., Y.Z., and S.G. performed the simulations. All authors discussed the results and commented on the manuscript.

Competing interests

The authors declare no competing interests.

Additional information

Supplementary information The online version contains supplementary material available at https://doi.org/10.1038/s41467-024-55512-3.

Correspondence and requests for materials should be addressed to Jie Jiang, Yueyu Zhang, Lei Zhang or Liang Chen.

Peer review information *Nature Communications* thanks the anonymous reviewer(s) for their contribution to the peer review of this work. A peer review file is available.